
Article:
Cerveny, M., Ford, K.L. orcid.org/0000-0002-1080-6193 and Tennant, A. (2021) Reflective switchable polarisation rotator based on metasurface with PIN diodes. IEEE Transactions on Antennas and Propagation, 69 (3). pp. 1483-1492. ISSN 0018-926X

https://doi.org/10.1109/tap.2020.3026883

Reflective Switchable Polarisation Rotator Based on Metasurface with PIN Diodes

Michal Cerveny, Kenneth Lee Ford, Alan Tennant

***Abstract*—A planar metasurface that rotates the polarisation of reflected signals by 90° is presented in this article. The surface also permits the relative phase of the rotated, reflected signal to be controlled. The metasurface rotator uses a square printed patch element mounted above a conducting ground plane. The addition of PIN diode controlled VIAs (Vertical Interconnect Access) at the corners of each square patch provide the ability to modify the scattering properties of the surface. In particular, the surface can be programmed to shift the phase of the rotated waveform by +/-90°. The polarisation rotator was manufactured, measured and compared against numerical simulations and the maximum measured bandwidth was 25% (4.8-6.2 GHz) for co-polarised attenuation of 10 dB. The proposed surface can be adopted for practical applications such as circularly polarised antennas.**

***Index Terms*—Polarisation rotator, Metasurface, Polarisation conversion**

I. Introduction

POLARISATION rotators have been investigated intensively for decades and there are many principles and geometries developed for polarisation conversion. One of the most common device based on polarisation rotation and used in daily life are liquid-crystal displays (LCD) [1], [2]. Even though the physical principles are the same for both optical and microwave spectrum [3]–[5], the practical challenges differ. Polarisation rotators can be further divided into two main categories: transmissive [6] and reflective [7]. This paper deals with a reflective switchable polarisation rotator designed for microwave frequencies. One of the most popular reflective polarisation rotator is based on split rings that have several modifications such as double split ring resonator for broadband characteristic [8], [9]. Moreover, triangular split ring resonator [10], L-shaped rotator [11] or substrate integrated waveguide cavity resonator [12] have been studied. Another group of polarisation rotators is based on metasurfaces utilising VIAs that connect a patch with ground plane [13]–[18]. All structures have one common similarity which is the type of symmetry. The structures are usually symmetric at the angle of 45°, so the surface can interact with linearly polarised waves oriented vertically or horizontally.

Also published are several active polarisation rotators based on tunable metasurface with varactor diodes [15] or with PIN diodes that allow switching the polarisation conversion on and off [19], [20].

In this paper, a reflective microwave metasurface that is capable of rotating the polarisation and also changing the reflected phase between two states was designed. In particular the phase difference between those two states of the reflected electromagnetic wave is 180°. Even though the proposed polarisation rotator uses a similar geometry as the one presented in [19], the functionality is different. The mentioned metasurface is capable of switching the polarisation rotation on and off but it does not have any capability to control/modulate the phase of rotated polarisation and the incident field must be oriented at the angle of 45°. Furthermore, the surface is capable to change the phase of co-polar reflection (unrotated polarisation) by 180° for x-polarised incident wave at a single frequency. That feature is useful especially when each unit cell can be addressed independently for adaptive beamstearing.

In contrast, the proposed metasurface is capable of switching the polarisation rotation on and off but at the same time the phase of the rotated polarisation can be controlled. The 180° phase difference is obtained not only at a single frequency but across the usable band. Finally, the incident field can be both vertically and horizontally polarised. The disadvantage of the proposed metasurface is that each unit cell cannot be independently addressed. This issue is discussed further in the article with possible solutions.

The functionality of a polarisation rotator in combination with the switchable phase change of 180° increases the practical usage greatly. For instance, it can be used for switchable circularly/linearly polarised antennas for satellite communication which allow the minimization of Faraday's effect and increase of polarisation diversity at the same time. This leads to higher spectral efficiency and reduced signal leakage due to polarisation mismatch and thus there is higher link reliability [21], [22]. The promoted polarisation rotator can also be used as a polarisation modulator [23], [24]. Also, secure wireless communication systems [25], [26] could benefit from this design. Another application is beamforming [27]. Overall, the proposed metasurface offers an alternative for cases where both polarisation rotation and a phase control are required.

The electromagnetic simulations were performed using full-wave analysis in the frequency domain considering unit cell boundary conditions in CST Microwave Studio. The results were validated by manufacturing and measuring both passive and active polarisation rotators.

The paper is structured as follows. Section II summarises the theory and presents the used notation. Section III studies several geometries of a passive rotator and measured results of the manufactured metasurface are compared with the simulations. Section IV deals with our design of an active polarisation rotator based on the principles presented in Section III. Section V shows a possible use of the metasurface.

M. Cerveny, K. L. Ford and A. Tennant were with the Department of Electronic and Electrical Engineering, The University of Sheffield, Sheffield, UK, e-mail: m.cerveny@sheffield.ac.uk.

II. Theory

In general, the reflection coefficient is defined as a ratio between the scattered field E^s and incident field E^i:

$$r = \frac{E^s}{E^i} \tag{1}$$

For simplicity, the electric field is considered as a plane wave propagating in z direction:

$$E = \hat{u}^{pol} E_0 e^{-j(kz-\omega t)} \tag{2}$$

where $\hat{u}^{pol}$ is the polarisation direction, E_0 is the magnitude of electric field, k is the wave number ($2\pi/\lambda$) and ω is the angular frequency ($2\pi f$). Electric field E can be decomposed into two orthogonal polarisations and the scattering matrix S is defined as:

$$\begin{bmatrix} E_x^s \\ E_y^s \end{bmatrix} = \begin{bmatrix} S_{xx} & S_{xy} \\ S_{yx} & S_{yy} \end{bmatrix} \begin{bmatrix} E_x^i \\ E_y^i \end{bmatrix} \tag{3}$$

In this case the electric field is oriented along the x- and y-axes. The components S_{xx} and S_{yy} are called co-polarised reflection coefficients and similarly, S_{yx} and S_{xy} are cross-polarised reflection coefficients. The co-polarised reflection coefficients are defined as:

$$r_{xx} = \frac{E_x^s}{E_x^i} \qquad r_{yy} = \frac{E_y^s}{E_y^i} \tag{4}$$

and the cross-polarised reflection coefficients are defined as:

$$r_{yx} = \frac{E_y^s}{E_x^i} \qquad r_{xy} = \frac{E_x^s}{E_y^i} \tag{5}$$

where E_x^i, E_y^i is the incident x-polarised, y-polarised electric field, respectively, and E_x^s, E_y^s is the scattered x-polarised, y-polarised electric field [28].

III. Study of Passive Polarisation Rotator

A polarisation rotator based on VIA connecting a top patch with a ground plane [13] was studied and modified (Fig. 1). It was assumed that by changing the position of the VIA from one corner of the patch to the other one, the surface currents induced by the incoming electromagnetic wave would be forced to change their direction and thus the vector of the rotated electromagnetic field should have the same magnitude but the opposite sign (direction). Thus, the change of position of VIA should provide phase difference of 180° of the reflected wave.

State A and B in Fig. 1 define the position of the VIA (right or left) and simulate an ideal switch. The physical dimensions of the rectangular unit cell are as follows, the width w is 9.4 mm, thickness of the dielectric h (FR-4, $\epsilon_r = 4.3$) is 6.4 mm and the length of each side of the patch l is 5.4 mm. The diameter of VIA is 0.8 mm.

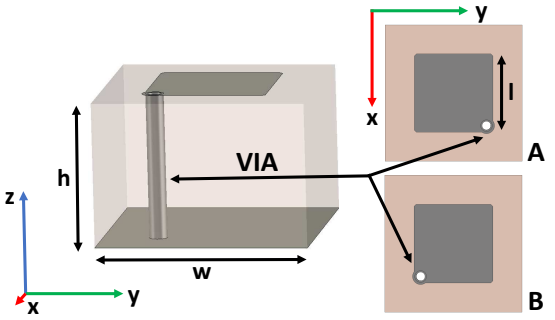

Fig. 1: Unit cell design of a passive rotator, state A: VIA is located on the right, state B: VIA is located on the left.

The diagonal symmetry allows the studied surface to be sufficient for both vertical and horizontal polarisation. As it is shown in Fig. 2, the passive rotator was tuned around the center frequency of 4.5 GHz where the cross-polarised reflection (red curve) and co-polarised reduction (blue curve) can be observed. Furthermore, state A and B does not have any effect on the magnitude of the reflection coefficient.

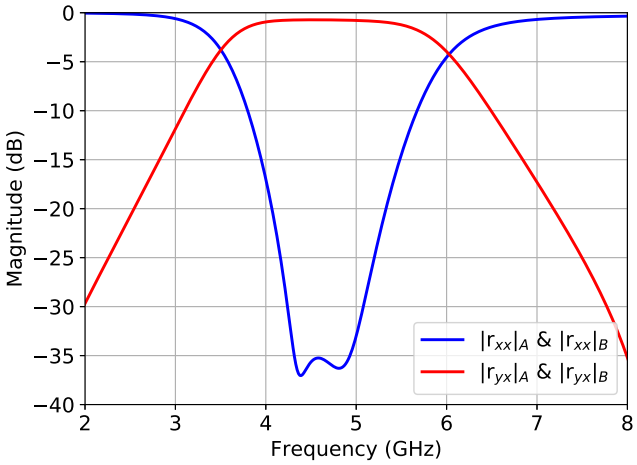

Fig. 2: Magnitude of the reflection coefficient for x-polarised wave at normal incidence (simulation).

A. Measurement

The measurement was performed in an anechoic chamber equipped with an NRL (Naval Research Laboratory) Arch which is a free-space measurement system for testing the reflectivity of materials. As shown in Fig. 3, it is equipped with two single polarised horn antennas oriented towards the metasurface. Furthermore, the antennas can be rotated by 90° which allows both co-polarised and cross-polarised measurements. For normal incidence, this configuration does not allow the pure monostatic measurement due to the width of the antennas. Therefore, the antennas are located close to each other to keep the bistatic angle as low as possible [28]. The physical separation between the horn antennas was approximately 1 cm. The antennas were connected by coaxial cables to Hewlett Packard 8720D network analyzer placed outside the chamber.

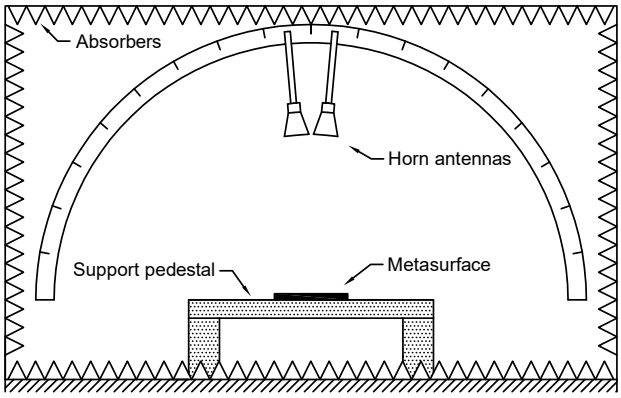

Fig. 3: NRL Arch - measurement setup.

For co-polarised measurement the bottom layer (flat plate) of the metasurface was used for calibration, so the reference plane was established at the front face of the metasurface. A long thin rod rotated by 45° in xy plane was used as a reference for the cross-polarised measurement. In the calibration procedure the empty chamber (isolation) was also taken into account. Furthermore, time gating was used for reduction of antenna coupling and residual reflections in the anechoic chamber.

Fig. 4 shows the manufactured metasurface. Dimensions of the PCB (Printed Circuit Board) were 404 x 404 mm and it consisted of 1849 unit cells, which were periodically placed in 43 columns and 43 rows. Top patches were connected with the bottom ground plane with VIAs. The diameter of VIAs (0.8 mm) was chosen based on our PCB manufacturer and its technical requirements.

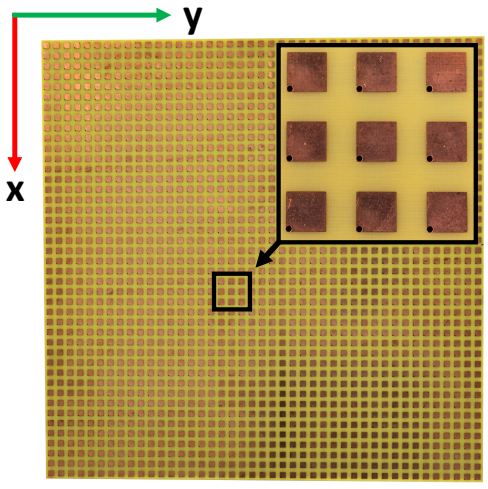

Fig. 4: Manufactured passive polarisation rotator.

The results are shown in Fig. 5. Subscripts A and B indicate the position of VIAs (right or left) for both measurement and simulation. (The surface had to be physically rotated by 90° to get from state A to state B.) It can be seen that the measurements of $|r_{xx}|_A$ and $|r_{xx}|_B$ differ even though the results should ideally be the same (as presented in the simulated results). The differences between the simulations and measurements can be caused by a few factors and most likely by their combination such as slightly curved surface, inhomogeneous substrate (FR-4), different permittivity of the substrate than it was considered in the simulation, non-constant thickness of the manufactured PCB and measurement error caused by physical rotation of the metasurface and due to the small bistatic angle of the horn antennas. On the other hand, this metasurface was made to prove the concept for our new design, so the small differences between our simulations and measurements were not an issue.

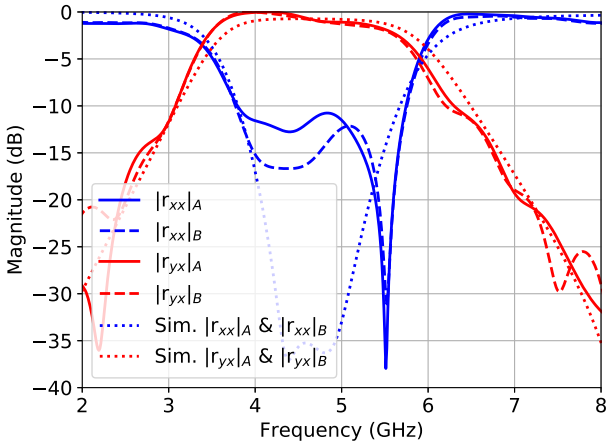

Fig. 5: Measured magnitude of the reflection coefficient for x-polarised wave at normal incidence for both state A and B. The simulated results are presented for comparison.

Fig. 6 shows the simulated and measured relative phase difference $\Delta\varphi$ between $r_{yx,A}$ and $r_{yx,B}$. The phase error of the measured surface was between 4° and 6° in the usable band in comparison to our results from simulation. In most of the practical applications the small phase error has a negligible effect on the performance.

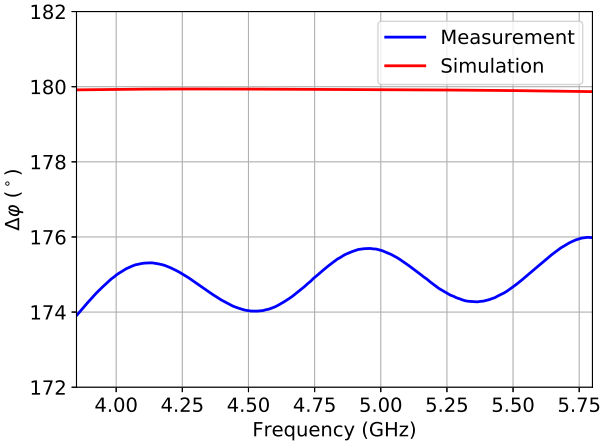

Fig. 6: Measured and simulated phase difference of the reflection coefficient between state A ($r_{yx,A}$) and B ($r_{yx,B}$).

The measured results proved that the rotated electromagnetic field is reflected in anti-phase when the state is changed from A to B and vice versa. This principle is further used for the design of a switchable metasurface.

B. Geometry of the polarisation rotator

This section deals with the shape of the top patch in terms of the overall performance of the rotator. As can be seen in Fig. 7 four different shapes were compared.

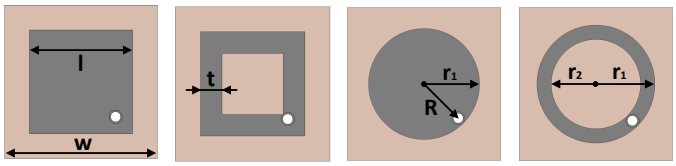

(a) Rotator 1 (b) Rotator 2 (c) Rotator 3 (d) Rotator 4

Fig. 7: Study of four geometries of the top patches and their effect on the performance of polarisation rotation.

The physical dimensions (unit cell) of the studied rotators were as follows, the width (w) was 9.1 mm and thickness of the grounded dielectric was 5.5 mm. The length (l) of each side of the square patch (Fig. 7a) was 6.1 mm and the thickness (t) of the square loop (Fig. 7b) was 1.3 mm. The radius (r_1) of the circular patch (Fig. 7c) was 3.5 mm and the inner radius (r_2) of the circular loop (Fig. 7d) was 2.65 mm. Position of the connection with ground plane can be seen as the white dots which were placed 3 mm away from the centre (R). The diameter of VIA was the same for all four unit cells (0.8 mm).

The polarisation rotator takes advantage of multiple resonances, which can be carefully tuned. Every resonance has limited bandwidth given by the Q-factor of the structure. Therefore, the overall usable bandwidth is determined by the requirements on the conversion ratio. The greater the conversion ratio is required, the narrower bandwidth can be expected. In this case three resonances were tuned close to each other to get one compact band with a high attenuation of the co-polarised reflection rather than having several single frequencies. Tuning can be performed by changing the physical dimensions of the unit cell and the position of VIA. The results from the simulations are presented in Fig. 8.

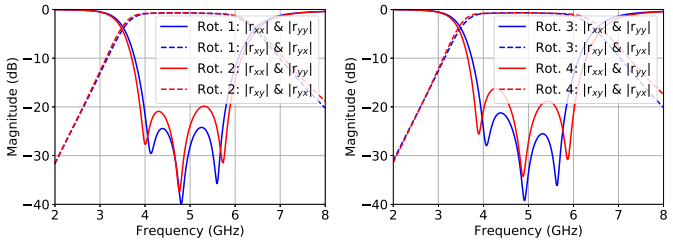

(a) Rotator 1 and 2 (b) Rotator 3 and 4

Fig. 8: Simulation of magnitude of the reflection coefficient at normal incidence for all four geometries of the top patches.

It can be seen that if the patch (rectangular or circular) is modified to a loop, the rotator with loop is slightly more broadband but the co-polarised attenuation is decreased approximately by 5 dB.

Based on these simulations we concluded that the shape of the top patch is not critical in terms of the response of the rotator and that the main functionality is provided by the position of VIA which creates an asymmetry allowing polarisation rotation.

C. Resonant modes of passive polarisation rotator

For better understanding of the converting mechanism, Fig. 9 shows the averaged surface currents for three resonant frequencies of Rotator 1. The rotator worked as a resonation circuit that was energized by $y(x)$-polarised incident field. An electric field oriented in z direction was created between the top patch and ground. Its averaged intensity correlated with the presented time-averaged current distributions. VIA placed in the corner of the patch created different potentials between neighbouring patches in the $x(y)$ direction. This effect can be seen in Fig. 10 where the surface was illuminated by y-polarised plane wave while the x component of the electric field appears between the top patches. This mechanism allowed to re-radiate the incident fields into the opposite polarisation.

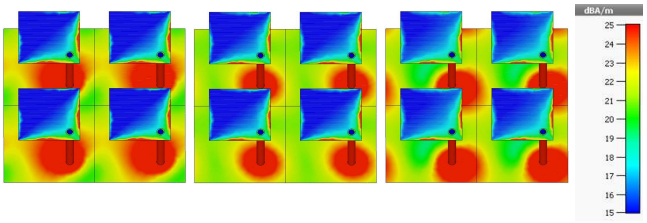

(a) 4.1 GHz (b) 4.8 GHz (c) 5.6 GHz (d) Scale

Fig. 9: Surface currents (averaged) presenting three resonant modes at frequency (a) 4.1 GHz, (b) 4.8 GHz and (c) 5.6 GHz. The scale is presented in (d).

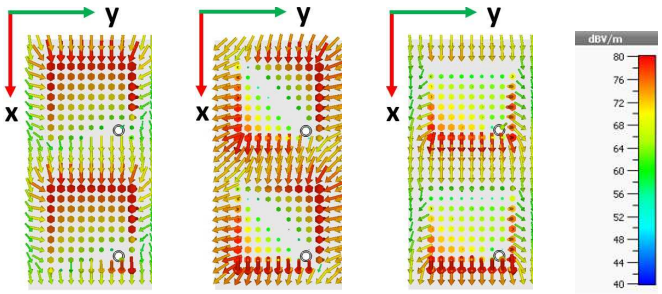

(a) 4.1 GHz (b) 4.8 GHz (c) 5.6 GHz (d) Scale

Fig. 10: E-filed plot presenting three resonant modes at frequency (a) 4.1 GHz, (b) 4.8 GHz and (c) 5.6 GHz. The scale is presented in (d).

D. Angular sensitivity and parametric study

This section presents the co-polarised and cross-polarised reflection coefficients for the angle of incidence Θ from 20° to 60° (Fig. 11) for both transverse electric (TE) and transverse magnetic (TM) polarised plane waves. The plane of incidence corresponds to zy plane. As the angle of incidence Θ increases, a small shift towards the higher frequencies can be observed as well as reduction of the conversion ratio (Fig. 12).

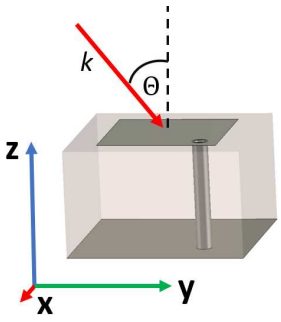

Fig. 11: Illustration of the incident angle Θ, k is the propagation vector and the plane of incidence corresponds to zy plane.

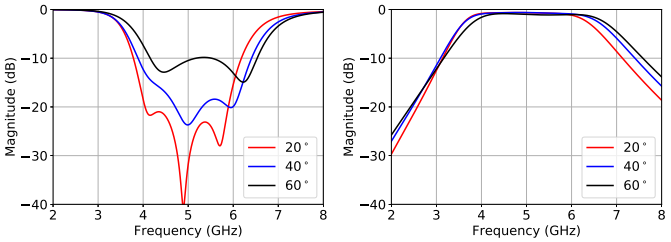

(a) TE co-polarisation (b) TE cross-polarisation

(c) TM co-polarisation (d) TM cross-polarisation

Fig. 12: Magnitude of reflection coefficients of Rotator 1 for the angle of incidence Θ from 20° to 60°.

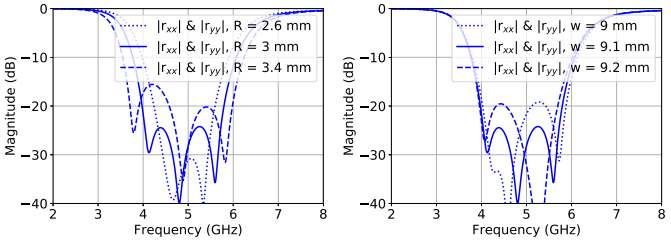

(a) Position of VIA (b) Width of unit cell

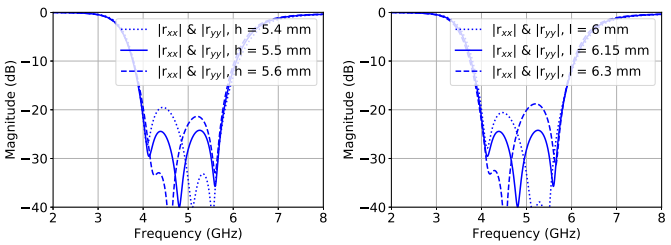

(c) Height of unit cell (d) Length of patch

Fig. 13: Magnitude of co-polarised reflection coefficients of Rotator 1, simulated results for different parameter values.

Furthermore, to see how the geometrical dimensions of the structure affect the resonant frequencies, a parametric study was performed.

Fig. 13a presents a parametric study for three distances (R) of VIA from the centre of the patch. It can be seen that with this parameter the overall bandwidth can be controlled. Moreover, the effect of adjusting the height (h), width of the unit cell (w) or length of the square patch (l) individually is presented in Fig. 13b-13d. In this case only co-polarised reflection coefficients are presented where the differences are more noticeable.

IV. Active Polarisation Rotator

Following the passive rotator, the analysis was extended to the reconfigurable case, which provides a number of practical challenges and is presented in this section.

A. Design and Simulations

Design of the active surface is based on the passive structure presented in the previous section. The aim was to modify the surface in such a way that the surface is capable of electrical rotation by 90° around its z-axis. This leads to the phase difference of the reflected wave of 180°.

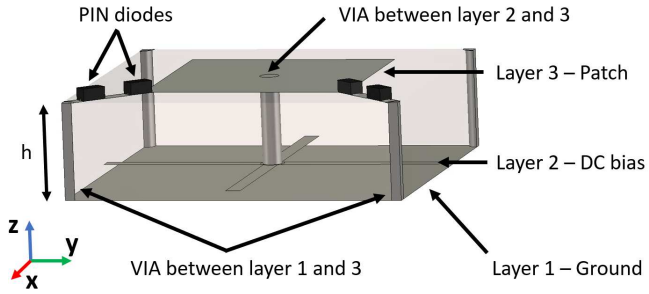

Fig. 14: Unit cell design of the switchable polarisation rotator. PIN diodes were simulated as RLC lumped elements and the black blocks (PIN diodes) were added for illustration purposes.

The metasurface was designed as a 3-layer PCB (Fig. 14) with the overall thickness h of the PCB 4 mm. The thickness between the bottom layer (Layer 1) and the middle one (Layer 2) was 0.4 mm and between the middle layer (Layer 2) and the top layer (Layer 3) was 3.6 mm. The blind VIA in the center of the unit cell worked as a DC bias and connected the top patch with Layer 2. Diameter of all VIAs was 0.8 mm.

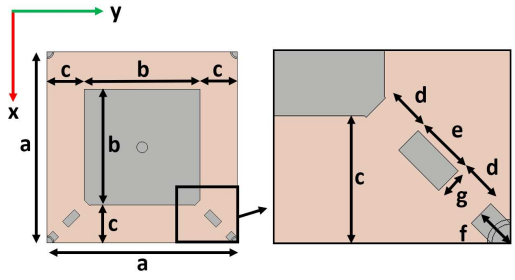

Fig. 15: Dimensions of the switchable polarisation rotator (top view).

Dimensions of the unit cell (Fig. 15) are shown in Tab. I. The top patch was placed to the centre of the unit cell and FR-4 substrate was considered for our design.

TABLE I: Dimensions of the switchable polarisation rotator.

Symbol	Dimension (mm)	Symbol	Dimension (mm)
a	14	b	8.5
c	2.75	d	1
e	1.24	f	0.9
g	0.6	h	4

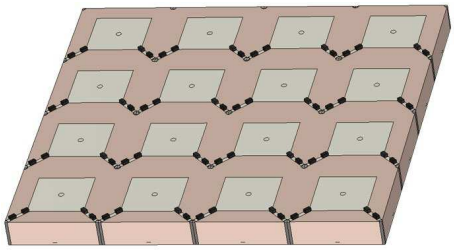

Fig. 16: Illustration of the metasurface containing 16 unit cells.

As can be seen the VIAs connected with ground (Layer 1) were moved into the corners of the unit cell. This allowed to share one VIA between two unit cells (Fig. 16) while only one patch was electrically connected to one VIA at a time. This solution simplified the design rapidly as each connection to the ground plane changed the field distribution on the metasurface.

PIN diodes were chosen for switching the structure as they are capable to provide large impedance changes at the frequencies of interest. Unfortunately, in comparison with an ideal switch they contain parasitic inductances, capacitances and resistances. This leads to finite isolation in OFF state and insertion losses in ON state. The PIN diodes were simulated as RLC lumped elements (Fig. 17). For ON state inductance L 0.6 nH and resistance R 2.1 Ω was considered. For OFF state inductance L 0.6 nH and capacitance C 0.17 pF was considered based on datasheet for PIN diode BAR64-02V.

(a) ON state (b) OFF state

Fig. 17: RLC equivalent circuits of PIN diode used in the simulations for ON and OFF state.

Fig. 18: Polarity of PIN diodes on the metasurface.

The electrical connection can be seen in Fig. 18. The diodes are connected with the central patch and with the ground plane through VIA located either on the right (state A) or on the left (state B). This design ensures that when diodes D1 and D2 are in ON state, diodes D3 and D4 are closed by a reverse voltage. It helps to obtain the correct functionality of the RF (Radio Frequency) switch as there is no floating voltage. Furthermore, because of the limited attenuation of PIN diodes in OFF state, two diodes were used in series, so the parasitic capacitance is halved. Hence the impedance of diodes D3 and D4 increases and so the isolation.

The simulated results are presented in Fig. 19a. It can be seen that the behaviour of the structure is slightly different for x- and y-polarised electromagnetic waves. The reason is that this structure unlike the passive one is not equal along x- and y-axis. It has a negligible effect on the rotated polarisation (cross-polarisation). Furthermore, the phase change of 180° was obtained across the entire usable band as shown in Fig. 19b.

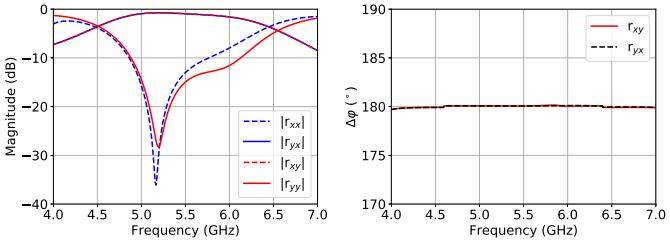

(a) (b)

Fig. 19: Simulated results: (a) Magnitude of the reflection coefficient at normal incidence. (b) Phase difference of the reflection coefficient between state A and B for both x- and y-polarised incident waves.

Fig. 20a shows the co-polarisation reflection coefficients for three values of parasitic capacitance of PIN diode. It can be seen that small difference of capacitance (0.2 pF) can change the resonation frequency of the polarisation rotator significantly. Fig. 20b presents the reflection coefficients when only one diode instead of two was used. When a design with only single diode was required, a single diode with a lower parasitic capacitance would need to be used. Typically, the smaller the parasitic capacitance of a PIN diode, the smaller the diode package, which can be difficult to solder without special tools.

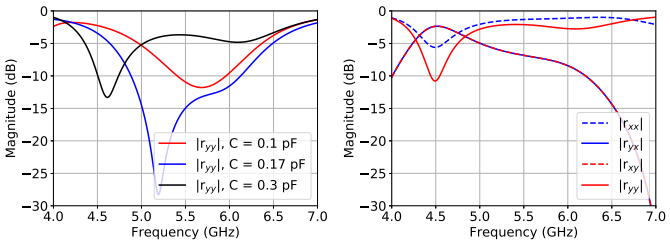

(a) (b)

Fig. 20: Simulated results: (a) Reflection coefficients $|r_{yy}|$ versus capacitance C used in the equivalent circuit. (b) Model with one diode considering capacitance of 0.17 pF.

Furthermore, a parametric study is presented in the following figures (Fig. 21a-21c) for $|r_{yy}|$. Reflection coefficients $|r_{xx}|$ work in the same way and therefore are not included. Practically, the design was limited by the dimensions of diodes. For example, the unit cell of width 13 mm would be preferable in terms of performance (Fig. 21b), but this unit cell would be too small for population of the diodes. For that reason a compromise had to be reached.

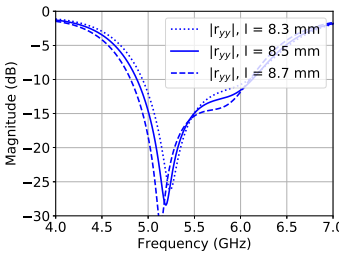

(a) Length of patch

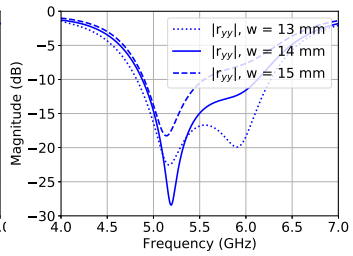

(b) Width of unit cell

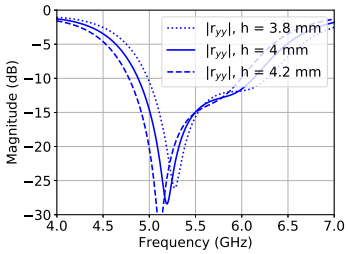

(c) Height of unit cell

Fig. 21: Simulated results for different parameter values of the switchable polarisation rotator.

B. Measurement

The proposed active polarisation rotator was manufactured (Fig. 22). It consisted of 121 unit cells located periodically in 11 rows and columns. The dimensions of the board were 16 x 16 cm.

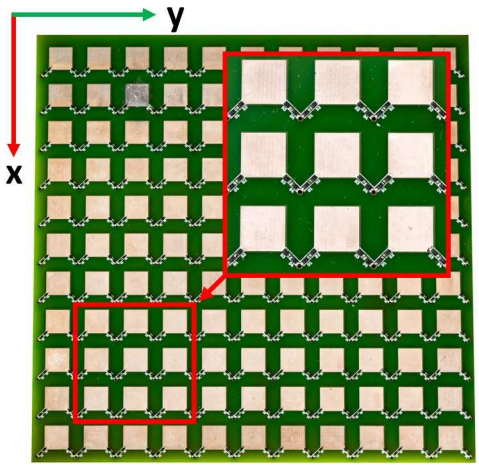

Fig. 22: Manufactured active polarisation rotator using three layer PCB and populated by PIN diodes (four PIN diodes per one unit cell).

It was measured for both x- (Fig. 23) and y-polarised (Fig. 24) incident fields. The magnitude of the reflection coefficients differs when the metasurface is switched from one state to the other. Ideally, the magnitude of the reflection coefficients should be the same for both polarities of the DC voltage. Practically, the difference can be observed especially in the co-polarised reflection. This effect is probably given by different resistance of the circuit as the current paths are different for each state. To compensate this effect, current levels would need to be set individually for state A and B. The metasurface can be switched from one state to the other with a very low current. The presented results are measured with total board current of 50 mA. The differences between the simulations and measurements could be introduced by manufacturing tolerances, measurement error and the simulation error caused especially by the simplified description of PIN diodes using an RLC equivalent circuit.

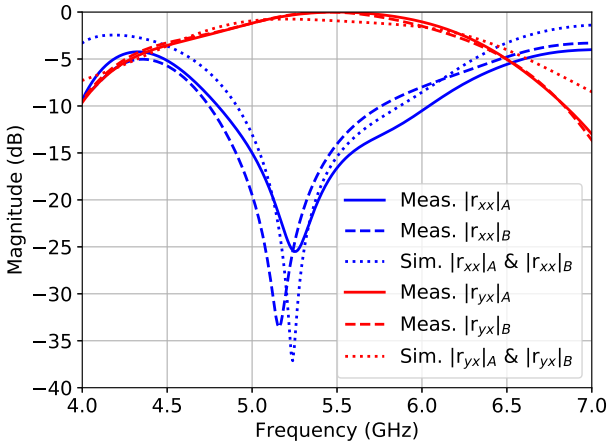

Fig. 23: Measured magnitude of the reflection coefficient for x-polarised wave at normal incidence for both state A and B. The simulated results are presented for comparison.

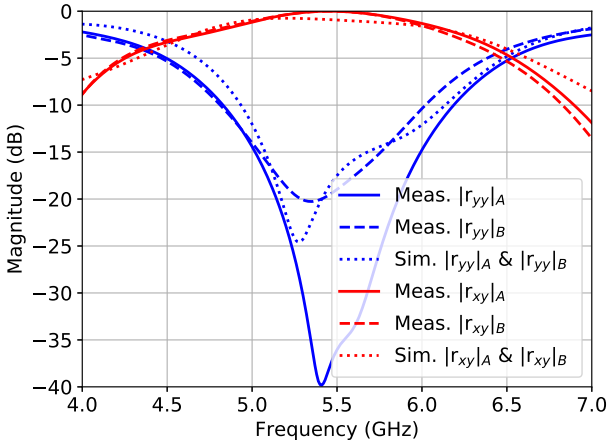

Fig. 24: Measured magnitude of the reflection coefficient for y-polarised wave at normal incidence for both state A and B. The simulated results are presented for comparison.

Fig. 25 shows the phase difference between state A and B for both x and y polarisations. The maximum phase error of the measured results was less than 5° for r_{xy} and 4° for r_{yx} in the frequency range from 4.5 GHz to 6.5 GHz in comparison to our simulation. This validated the simulated results and the

correct functionality of the designed switchable polarisation rotator.

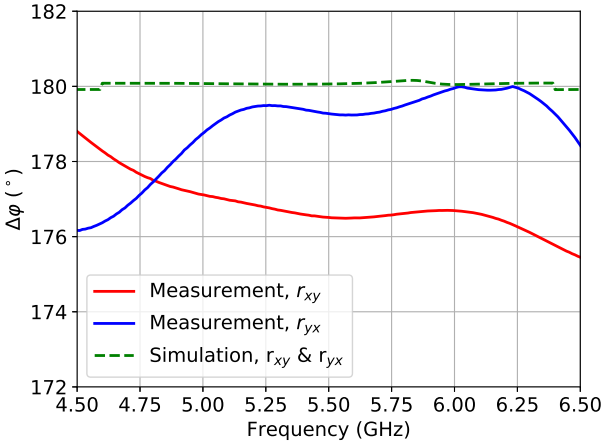

Fig. 25: Measured and simulated phase difference of the reflection coefficient between state A and B for both x- and y-polarised incident waves.

V. Switchable Polarisation Rotator Usage for Practical Applications

The presented metasurface can be further customised. In the previous section all the unit cells were connected together, so the entire metasurface could be changed from state A to state B just by changing the DC polarity and only two wires were needed for controlling the entire metasurface. This design can be easily modified for adaptive beamforming, so each line or row can be controlled independently based on the requirements (Fig. 26).

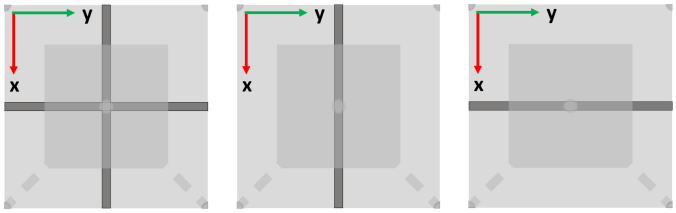

(a) XY (b) X (c) Y

Fig. 26: Possible configurations (XY, X, Y) of DC bias at the second layer.

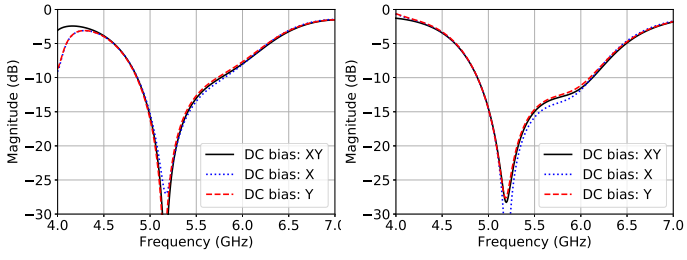

(a) $|r_{xx}|$ (b) $|r_{yy}|$

Fig. 27: Simulated magnitude (co-polarisation) of the reflection coefficient for three possible configurations (XY, X, Y) of the DC bias.

The DC bias placed in the metasurface has a negligible effect on the performance for both horizontally (y-axis) and vertically (x-axis) polarised incident fields (Fig. 27). The unit cells can further be grouped into clusters, so each cluster (super cell containing several unit cells) can be controlled independently.

A practical use of the proposed active metasurface can be an active antenna or modulator that can switch between right-hand/left-hand circular polarisation (RHCP/LHCP) as well as linear polarisation (LP). To obtain a circular polarisation, two components (vertical and horizontal) must exist with the phase difference of 90°. This can be achieved by placing a simple dipole antenna in front of the metasurface. As the rotator was designed for plane-wave interaction, the dipole of length 21 mm was placed 600 mm (12.2 λ at 6.1 GHz) in front of the metasurface to be in the far-field region. The change of RHCP/LHCP and LP radiation pattern can be done only by applying the respective DC voltage to the metasurface.

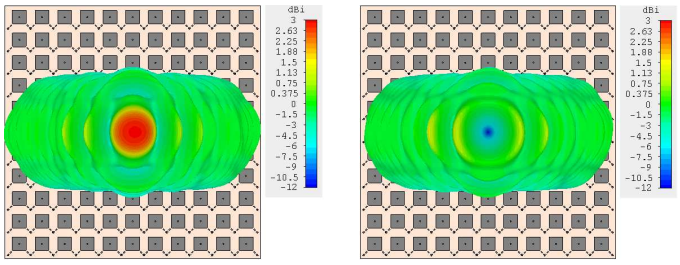

(a) RHCP (b) LHCP

Fig. 28: State A: (a) RHCP and (b) LHCP far-field radiation pattern at 6.1 GHz. The central top patch was connected with the VIA on the right side. RHCP main beam was produced.

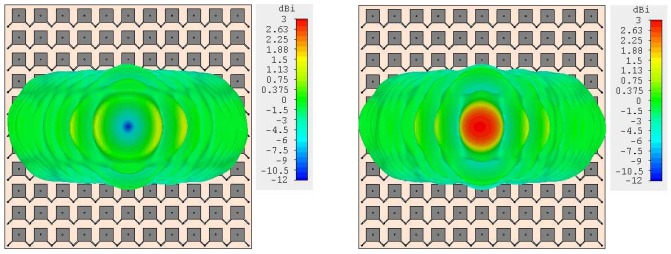

(a) RHCP (b) LHCP

Fig. 29: State B: (a) RHCP and (b) LHCP far-field radiation pattern at 6.1 GHz. The central top patch was connected with the VIA on the left side. LHCP main beam was produced.

Fig. 28 shows the radiation pattern for state A. It can be seen that this state produced RHCP polarisation while LHCP polarisation was highly attenuated. When the state is switched from state A to state B, LHCP polarisation was radiated into the required direction while RHCP is now attenuated (Fig. 29).

The ratio between the circular polarisations for each state is shown in Fig. 30. It can be seen that the highest ratio occurs in the direction of the main beam. This feature may be attractive

for secure wireless communications where the transmitted signal can be correctly decoded only in the direction of the main beam.

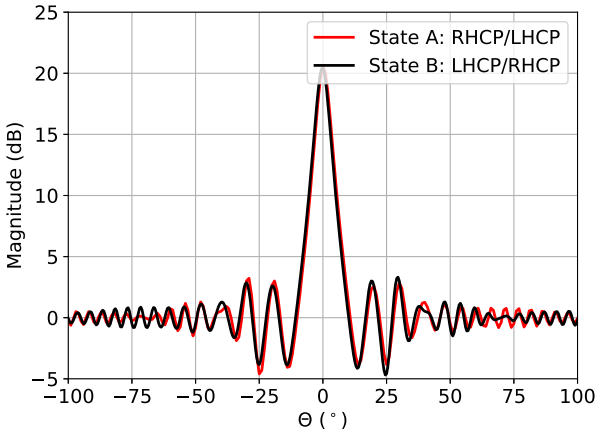

Fig. 30: Ratio RHCP/LHCP for state A and LHCP/RHCP for state B.

Furthermore, when no current is applied, the metasurface behaves as a regular reflector without any rotating functionality. This off state is presented in Fig. 31. As the dipole was vertically polarised in front of the metasurface, the whole antenna system with the metasurface produced only linear polarisation (vertical).

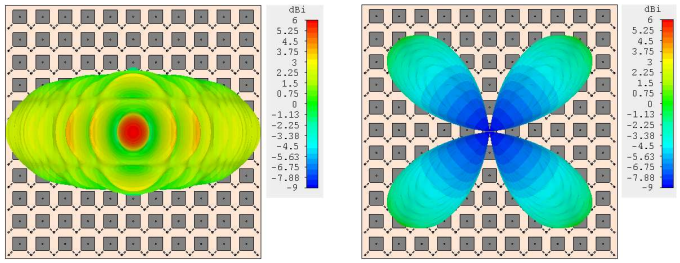

(a) Vertical polarisation (b) Horizontal polarisation

Fig. 31: Metasurface in off state illuminated by vertically-polarised wave (dipole antenna).

VI. Conclusion

In this article, a reflective switchable polarisation rotator based on an artificial magnetic conductor with offset VIA was presented. Following the study of electromagnetic properties and the effect of different topologies of a passive polarisation rotator, the analysis was extended to the reconfigurable case. The final design was capable of rotating the polarisation by 90° and switching the relative phase of the reflected electromagnetic wave by 180°. Furthermore, the surface allowed to behave as a regular conductive reflector in off state. The main advantage of our design is the fact that the phase of the rotated, reflected electromagnetic wave can be controlled. The relative phase difference of 180° was obtained not only at a single frequency but across the entire usable band for both vertically and horizontally polarised incident fields.

Based on our simulations and measurements, the surface worked in the frequency range of 4.8 and 6.2 GHz for co-polarised attenuation of 10 dB and the overall maximum measured phase error of the rotator was better than 4° in the usable bandwidth for both polarisations.

In combination with a simple dipole antenna, a switchable antenna with right hand circular polarisation, left hand circular polarisation and linear polarisation can be achieved. This can be advantageous for polarisation diversity as well as for design of a polarisation modulator.

The metasurface can be further customised for beamforming capability by splitting the metasurface into several independently controlled sections. Also, this surface could provide polarisation scrambling useful for secure wireless communication systems. Overall, the presented metasurface offers an alternative for cases where both polarisation rotation and a phase control are required.

References

[1] Xinyu Zhu, Zhibing Ge, T. X. Wu, and Shin-Tson Wu, "Transflective liquid crystal displays," *Journal of Display Technology*, vol. 1, no. 1, pp. 15–29, 2005.

[2] Hyungki Hong, "Dependency of spectral reflectance on rotating direction of liquid crystal for reflective liquid crystal displays," *Journal of Display Technology*, vol. 2, no. 3, pp. 233–236, 2006.

[3] A. Overvig, S. Shrestha, S. Malek, M. Lu, A. Stein, C. Zheng, and N. yu, "Dielectric metasurfaces for complete and independent control of the optical amplitude and phase," *Light: Science & Applications*, vol. 8, p. 92, 10 2019.

[4] S. Gao, C.-S. Park, S.-S. Lee, and D.-Y. Choi, "All-dielectric metasurfaces for simultaneously realizing polarization rotation and wavefront shaping of visible light," *Nanoscale*, vol. 11, pp. 4083–4090, 2019.

[5] X. Zhang, S. Yang, W. Yue, Q. Xu, C. Tian, X. Zhang, E. Plum, S. Zhang, J. Han, and W. Zhang, "Direct polarization measurement using a multiplexed pancharatnam–berry metahologram," *Optica*, vol. 6, pp. 1190–1198, Sep 2019.

[6] Z. Wu, Y. Ra'di, and A. Grbic, "Tunable metasurfaces: A polarization rotator design," *Phys. Rev. X*, vol. 9, p. 011036, Feb 2019.

[7] S. Yu, L. Li, G. Shi, C. Zhu, X. Zhou, and Y. Shi, "Design, fabrication, and measurement of reflective metasurface for orbital angular momentum vortex wave in radio frequency domain," *Applied Physics Letters*, vol. 108, no. 12, p. 121903, 2016.

[8] S. J. Li, X. Y. Cao, L. M. Xu, L. J. Zhou, H. H. Yang, J. F. Han, Z. Zhang, D. Zhang, X. Liu, C. Zhang, Y. J. Zheng, and Y. Zhao, "Ultra-broadband reflective metamaterial with rcs reduction based on polarization convertor, information entropy theory and genetic optimization algorithm," *Scientific Reports*, 2016.

[9] C. Hong-Ya, W. Jia-Fu, M. Hua, Q. Shao-Bo, Z. Jie-Qiu, X. Zhuo, and Z. An-Xue, "Broadband perfect polarization conversion metasurfaces," *Chinese Physics B*, vol. 24, no. 1, p. 014201, 2015.

[10] Q. Zheng, C. Guo, H. Li, and J. Ding, "Wideband and high efficiency reflective polarization rotator based on metasurface," *Journal of Electromagnetic Waves and Applications*, vol. 32, no. 3, pp. 265–273, 2018.

[11] Y. Jia, Y. Liu, W. Zhang, and S. Gong, "Ultra-wideband and high-efficiency polarization rotator based on metasurface," *Applied Physics Letters*, vol. 109, no. 5, p. 051901, 2016.

[12] X. C. Zhu, W. Hong, K. Wu, H. J. Tang, Z. C. Hao, J. X. Chen, and G. Q. Yang, "A novel reflective surface with polarization rotation characteristic," *IEEE Antennas and Wireless Propagation Letters*, vol. 12, pp. 968–971, 2013.

[13] D. Yan, Q. Gao, C. Wang, C. Zhu, and N. Yuan, "A novel polarization convert surface based on artificial magnetic conductor," in *2005 Asia-Pacific Microwave Conference Proceedings*, vol. 3, pp. 2 pp.–, Dec 2005.

[14] M. H. Ghazizadeh, G. Dadashzadeh, and M. Korshidi, "A novel wideband electromagnetic band gap structure for circular polarization conversion," in *2012 15 International Symposium on Antenna Technology and Applied Electromagnetics*, pp. 1–4, June 2012.

[15] W. Yang, D. Chen, W. Che, and W. Feng, "Multi-functional antennas using polarization-rotation artificial magnetic conductor structures," in *2017 10th Global Symposium on Millimeter-Waves*, pp. 11–14, May 2017.

[16] W. Yang, K. W. Tam, W. W. Choi, W. Che, and H. T. Hui, "Novel polarization rotation technique based on an artificial magnetic conductor and its application in a low-profile circular polarization antenna," *IEEE Transactions on Antennas and Propagation*, vol. 62, pp. 6206–6216, Dec 2014.

[17] W. Yang, K. W. Tam, W. W. Choi, W. Che, and H. T. Hui, "Polarisation rotation reflective surface based on artificial magnetic conductor and its application," *Electronics Letters*, vol. 50, pp. 1500–1502, October 2014.

[18] W. Yang, W. Che, W. W. Choi, and K. W. Tam, "A low-profile circularly polarized dipole antenna using a novel polarization rotation artificial magnetic conductor," in *2014 44th European Microwave Conference*, pp. 374–377, Oct 2014.

[19] H. Yang, X. Cao, F. Yang, J. Gao, S. Xu, M. Li, X. Chen, Y. Zhao, Y. Zheng, and L. Sijia, "A programmable metasurface with dynamic polarization, scattering and focusing control," *Scientific Reports*, vol. 6, 10 2016.

[20] M. Saikia, S. Ghosh, and K. V. Srivastava, "Switchable reflective metamaterial polarisation rotator," *Electronics Letters*, vol. 52, no. 12, pp. 1030–1032, 2016.

[21] I. Gheorghisor, A. Dissanayake, J. Allnutt, and S. Yaghmour, "Prediction of faraday rotation impairments in c-band satellite links," in *IEEE Antennas and Propagation Society International Symposium. Transmitting Waves of Progress to the Next Millennium. 2000 Digest. Held in conjunction with: USNC/URSI National Radio Science Meeting (C*, vol. 2, pp. 554–557 vol.2, 2000.

[22] H. Yang, J. An, H. Jung, J. Kim, and J. T. S. Sumantyo, "Circular polarization implementation on synthetic aperture radar," in *2014 International Conference on Information and Communication Technology Convergence (ICTC)*, pp. 991–994, 2014.

[23] I. Toyoda, *Modulation in Electronics and Telecommunications*, ch. Polarization Modulation. 07 2019.

[24] S. Henthorn, K. L. Ford, and T. O'Farrell, "Frequency selective surface loaded antenna for direct antenna modulation," in *2017 11th European Conference on Antennas and Propagation (EUCAP)*, pp. 731–734, 2017.

[25] Z. Luo, H. Wang, and W. Lv, "Directional polarization modulation for secure transmission in dual-polarized satellite mimo systems," in *2016 8th International Conference on Wireless Communications Signal Processing (WCSP)*, pp. 1–5, 2016.

[26] X. Zhang, B. Zhang, and D. Guo, "Physical layer secure transmission based on fast dual polarization hopping in fixed satellite communication," *IEEE Access*, vol. 5, pp. 11782–11790, 2017.

[27] L. Di Palma, A. Clemente, L. Dussopt, R. Sauleau, P. Potier, and P. Pouliguen, "Radiation pattern synthesis for monopulse radar applications with a reconfigurable transmitarray antenna," *IEEE Transactions on Antennas and Propagation*, vol. 64, no. 9, pp. 4148–4154, 2016.

[28] E. K. . J. S. . M. Tuley, *Radar Cross Section*. SciTech Publishing, 2004.

[29] Z. Zhang, X. Cao, J. Gao, and S. Li, "Broadband metamaterial reflectors for polarization manipulation based on cross/ring resonators," *Radioengineering Journal*, pp. 436–441, 2016.

[30] B. Lin, B. Wang, W. Meng, X. Da, W. Li, Y. Fang, and Z. Zhu, "Dual-band high-efficiency polarization converter using an anisotropic metasurface," *Journal of Applied Physics*, vol. 119, no. 18, p. 183103, 2016.

[31] H. F. Ma, G. Z. Wang, G. S. Kong, and T. J. Cui, "Broadband circular and linear polarization conversions realized by thin birefringent reflective metasurfaces," *Opt. Mater. Express*, vol. 4, pp. 1717–1724, Aug 2014.

[32] H. Chen, J. Wang, H. Ma, S. Qu, Z. Xu, A. Zhang, M. Yan, and Y. Li, "Ultra-wideband polarization conversion metasurfaces based on multiple plasmon resonances," *Journal of Applied Physics*, vol. 115, no. 15, p. 154504, 2014.

[33] Y. Liu, K. Li, Y. Jia, Y. Hao, S. Gong, and Y. J. Guo, "Wideband rcs reduction of a slot array antenna using polarization conversion metasurfaces," *IEEE Transactions on Antennas and Propagation*, vol. 64, pp. 326–331, Jan 2016.

[34] J. Hao, Y. Yuan, L. Ran, T. Jiang, J. A. Kong, C. T. Chan, and L. Zhou, "Manipulating electromagnetic wave polarizations by anisotropic metamaterials," *Phys. Rev. Lett.*, vol. 99, p. 063908, Aug 2007.

[35] L. Zhang, P. Zhou, H. Lu, H. Chen, J. Xie, and L. Deng, "Ultra-thin reflective metamaterial polarization rotator based on multiple plasmon resonances," *IEEE Antennas and Wireless Propagation Letters*, vol. 14, pp. 1157–1160, 2015.

[36] Q. Zheng, C. Guo, H. Li, and J. Ding, "Broadband radar cross-section reduction using polarization conversion metasurface," *International Journal of Microwave and Wireless Technologies*, vol. 10, no. 2, p. 197–206, 2018.

[37] J. J. Yang, Y. Z. Cheng, C. C. Ge, and R. Z. Gong, "Broadband polarization conversion metasurface based on metal cut-wire structure for radar cross section reduction," *Materials*, 2018.

[38] M. Feng, J. Wang, H. Ma, W. Mo, H. Ye, and S. Qu, "Broadband polarization rotator based on multi-order plasmon resonances and high impedance surfaces," *Journal of Applied Physics*, vol. 114, no. 7, p. 074508, 2013.

[39] Y. Jia, Y. Liu, Y. J. Guo, K. Li, and S. X. Gong, "Broadband polarization rotation reflective surfaces and their applications to rcs reduction," *IEEE Transactions on Antennas and Propagation*, vol. 64, pp. 179–188, Jan 2016.

[40] P. J. Ferrer, J. M. Gonzalez-Arbesu, C. Craeye, and J. Romeu, "Transpolarizing surfaces and potential applications," in *2008 38th European Microwave Conference*, pp. 281–284, Oct 2008.

[41] S. Henthorn, K. L. Ford, and T. O'Farrell, "Bit-error-rate performance of quadrature modulation transmission using reconfigurable frequency selective surfaces," *IEEE Antennas and Wireless Propagation Letters*, vol. 16, pp. 2038–2041, 2017.

[42] K. L. Ford, J. Roberts, S. Zhou, G. Fong, and J. Rigelsford, "Reconfigurable frequency selective surface for use in secure electromagnetic buildings," *Electronics Letters*, vol. 49, pp. 861–863, July 2013.

[43] A. Tennant, W. Hurley, and T. Dias, "Knitted, textile, high impedance surface with integrated conducting vias," *Electronics Letters*, vol. 49, pp. 8 –10, January 2013.

[44] W. Xu and S. Sonkusale, "Microwave diode switchable metamaterial reflector/absorber," *Applied Physics Letters*, vol. 103, 07 2013.

Michal Cerveny Received his M.Sc. from the Czech Technical University (CTU) in Prague in 2014 and is currently working towards his Ph.D. focused on controlling the propagation of electromagnetic waves using artificial materials. In 2014, he started to work as a visiting researcher at the University of Sheffield working on wireless friendly energy efficient buildings. In 2015, he worked for The Rolls-Royce University Technology Centre doing RF modelling within marine environments and since 2016 he has been working at The University of Sheffield as a research associate in applied electromagnetics.

Alan Tennant Received the B.Eng. degree in electronic engineering and the Ph.D. degree in medical physics, both from the Univerisity of Sheffield, Sheffield, U.K., in 1985, and 1992, respectively. Between 1985 and 1986, he worked with BAE Systems, Stevenage, U.K. In 1992, he joined Defence and Evaluation Research Agency (DERA), Malvern, U.K., where he worked on phased-array antenna systems, before taking up an academic post at the University of Hull, Hull, U.K. He returned to the Department of Electronic and Electrical Engineering, University of Sheffield, in 2001, as a Senior Lecturer in the Communications and Radar Group where he is involved in research into adaptive materials for radar signature management, novel three-dimensional phased array antenna topologies, and acoustic array systems.

Kenneth Lee Ford (M'07–SM'10) received the B.Eng. and Ph.D. degrees in electronic engineering from the University of Sheffield, Sheffield, U.K. in 1998 and 2003, respectively. In 2001, he joined the Stealth Materials Department, Advanced Technology Centre, BAE Systems, Towcester, U.K. In 2005, he joined the University of Sheffield as a Lecturer of communications, and became a Senior Lecturer in 2012. His current research interests include reconfigurable antennas, miniaturized antennas, metamaterials, propagation in the built environment, and electromagnetic structures for biomedical applications.